CDF/ANAL/EXOTIC/PUBLIC/8944
August 8, 2007
version 1.0

Search for Gluino and Squark Production in Multijets Plus Missing $\mathrm{E_T}$ Final States using 1.4 fb^{-1}

M. D'Onofrio, G. De Lorenzo, M. Martinez

(IFAE-Barcelona)

Abstract

We present an update on the analysis that searches for squarks and gluinos in proton-antiproton collisions with a center-of-mass energy of 1.96 TeV at the Tevatron: results are based on 1.4 fb^{-1} of data collected by the CDF detector in Run II. This note has to be considered as an addendum of CDFNotes 8751 and 8885. No excess with respect to Standard Model predictions is observed. In a mSUGRA scenario with $A_0 = 0$, $\mu < 0$ and $\tan\beta = 5$, we exclude masses up to about 380 $\mathrm{GeV/c^2}$ at 95% C.L. in the region where gluino and squark masses are similar, gluino masses up to 280 $\mathrm{GeV/c^2}$ for every squark mass, and gluino masses up to 410 $\mathrm{GeV/c^2}$ for squark masses below 375 $\mathrm{GeV/c^2}$.

1 Datasets

The analysis presented in this note is based on Run II data collected between 2002 and end of 2006. The run number is in the range 138809 - 228596 and the DQM GoodRun List v17 (0,0,0,0) is used. Within respect to notes [1] and [2], the analysis has been updated including data in run range [217990-228596] – so-called periods 8 and 9 of data-taking.

The three-level trigger logic employed to collect the event sample requires the presence of at least two jets in the final state together with large $\not\!\!E_T$ (MET35_&_TWO_JETS). Few changes have been introduced in the trigger logic along data-taking periods:

- after run 195739, at L2 one of the two trigger jets is required to be central in order to reduce beam-halo background and keep acceptable trigger rates (path name MET35_&_CJET_&_JET). This modification did not result in an efficiency loss in the analysis, since at least one central jet is required in the event selection.
- During data-taking period 8, the MET35 trigger has been lumi-enabled: the logic of the path is kept the same, but if the instantaneous luminosity is above 190 $\times 10^{30}$ $cm^{-2}s^{-1}$, the trigger is turned off (path name MET35_&_CJET_&_JET_LUMI_190).

Table 1 shows in detail the trigger requirements at the different levels.

Trigger Level	requirement	Prescale
L1	MET 25	1
L2	TWO-JET10 (CJET10-JET10) .and. L1-MET25	1
L3	MET 35	1

Table 1: Summary of the MET35 trigger logic used in collecting the data. In parenthesis the L2 selection after run 195739 is reported.

It should be noted that an high occupancy trigger tower [3] in the WHA region has been identified in data-taking period 8, masked after run 220727. Since the presence of such hot tower could strongly bias the trigger, data collected between runs 217990 and 220727 are not included in the analysis.

The integrated luminosities of data periods 8 (first part excluded) and 9 are found to be 109.7 and 169.6 pb^{-1}, respectively (correction factor 1.019 included). The total luminosity used in the analysis is then 1.37 fb^{-1}.

1.1 Data stability: MET35 path

No significant dependence of the measured cross section with the data-taking periods is observed between the first 1.1 fb^{-1} (periods 0-7) and periods 8 and 9. Some relevant variables are shown in figures 1 to 3: jet multiplicity, corrected $\not\!\!E_T$ and H_T, where H_T is defined as the sum of the corrected transverse energy of the first two leading jets. Each distribution is scaled to the corresponding luminosity of the data sample, and events are selected using the basic criteria as reported in section 5 of note 8885 [1], GoodRun List v17 (0,0,0,0), $|V_z| < 60$ cm, EEMF> 0.15, ECHF> 0.15, corrected $\not\!\!E_T > 70$ GeV and 2 jets with $E_T^{jet} > 25$ GeV and $|\eta^{jet}| < 2.$, with one central jet ($|\eta^{jet}| < 1.1$).

[1] Similar agreement is also obtained using 3-jets or 4-jets preselection requirements.

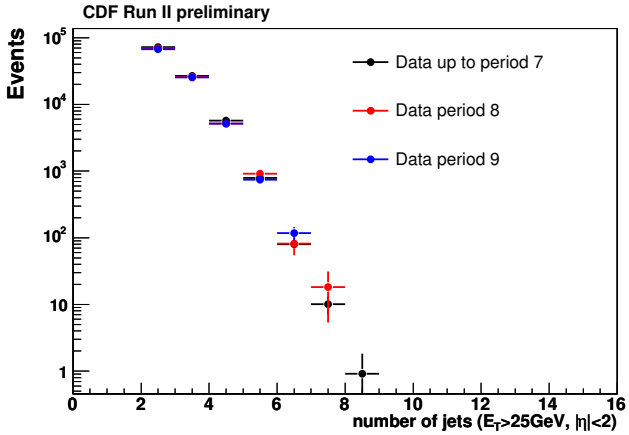

Figure 1: Number of jets with transverse energy above 25 GeV for data periods [0-7], 8 and 9. The plot includes all preselection cuts: GoodRun List v17 (0,0,0,0), EEMF> 0.15, ECHF> 0.15, $|V_z| < 60$ cm, corrected $\not\!\!E_T > 70$ GeV and 2 jets with $E_T^{jet} > 25$ GeV and $|\eta^{jet}| < 2$.

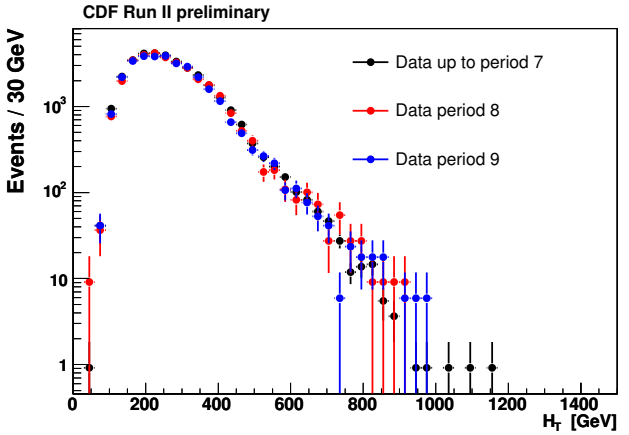

Figure 2: H_T distribution for data periods [0-7], 8 and 9. The plot includes all preselection cuts: GoodRun List v17 (0,0,0,0), $|V_z| < 60$ cm, EEMF> 0.15, ECHF> 0.15, corrected $\not\!\!E_T > 70$ GeV and 2 jets with $E_T^{jet} > 25$ GeV and $|\eta^{jet}| < 2$.

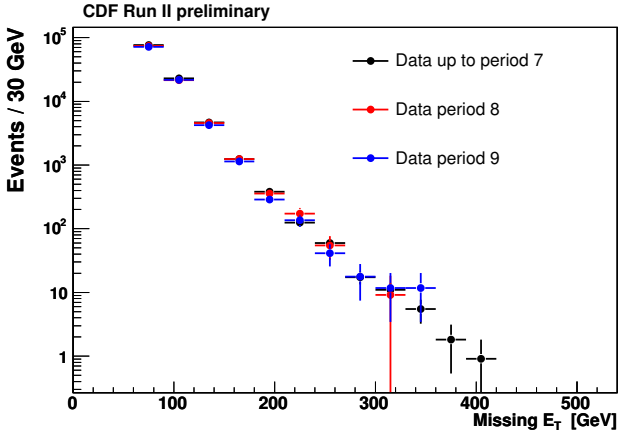

Figure 3: Corrected $\not\!\!E_T$ for data periods [0-7], 8 and 9. The plot includes all preselection cuts: GoodRun List v17 (0,0,0,0), $|V_z| < 60$ cm, EEMF> 0.15, ECHF> 0.15, corrected $\not\!\!E_T > 70$ GeV and 2 jets with $E_T^{jet} > 25$ GeV and $|\eta^{jet}| < 2$.

1.2 Control regions: reversed cuts

Control regions for 3- and 4-jets analyses are defined reversing as follows the selection cuts used to reject specific background contributions:

- $\Delta\phi(\text{jet}, \not\!\!\text{E}_\text{T})$ is required to be <0.7, for at least one of the three leading jets, or <0.3 for the fourth leading jet in case of 4-jets selection, to enhance the QCD background contribution.
- at least one of the three/four leading jets is required to have EMF>0.9, to enhance Boson+jets and Dibosons backgrounds, with electrons in the final state.
- one isolated track is required to be along $\not\!\!\text{E}_\text{T}$ ($\Delta\phi(\text{trk}, \not\!\!\text{E}_\text{T})$ <0.7), or two isolated tracks are required to have invariant mass within the Z mass window range ($76 < \text{M(inv)} < 106$ GeV/c^2). This selection enhances muon-related contributions, in particular Boson+jets and top backgrounds.

Figures 4 to 6 show the N-1 distributions for $\not\!\!\text{E}_\text{T}$ and H_T, after all selection cuts according to the 3-jet (zone C as example) region with the different reversed cuts (total background and non-QCD background contributions are reported). Figures 7 to 9 show the N-1 distributions for $\not\!\!\text{E}_\text{T}$ and H_T according to the 4-jet region. Good agreement between data and Monte Carlo is found in all cases.

In the case of the 2-jet region, the requirements on $\not\!\!\text{E}_\text{T}$ and H_T are very tight. We use as control regions the data where all the selection cuts are applied but those on both $\not\!\!\text{E}_\text{T}$ and H_T (N-2 plots). Figure 10 show the distributions for $\not\!\!\text{E}_\text{T}$ (top) and H_T(bottom): good agreement is found within systematic uncertainties.

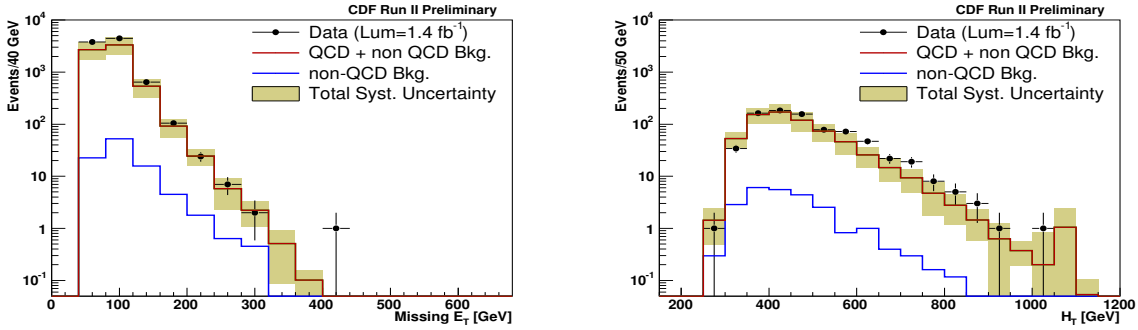

Figure 4: $\not\!\!E_T$ and H_T after all cuts in the 3-jet (zone C) analysis except the $\not\!\!E_T$ and H_T cuts respectively, but reversing the $\Delta\phi(\not\!\!E_T, \text{jets})$ cut by asking at least one of the jets to fail the condition. QCD and non-QCD background plus systematic uncertainties are shown.

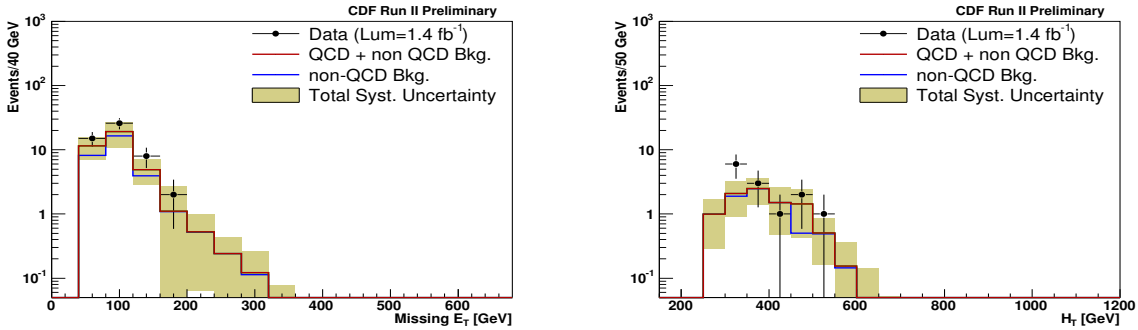

Figure 5: $\not\!\!E_T$ and H_T after all cuts in the 3-jet (zone C) analysis except the $\not\!\!E_T$ and H_T cuts respectively, but reversing the EMF requirement by asking at least one of four leading jets to fail the condition. QCD and non-QCD background plus systematic uncertainties are shown.

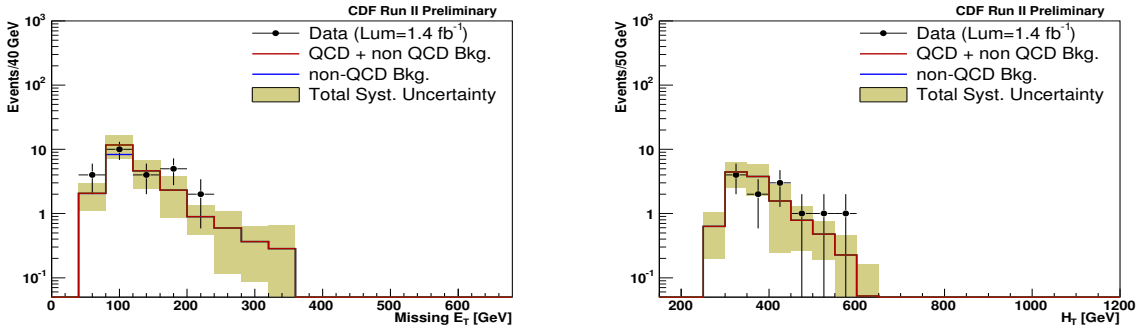

Figure 6: $\not\!\!E_T$ and H_T after all cuts in the 3-jet (zone C) analysis except the $\not\!\!E_T$ and H_T cuts respectively, but enhancing the muon contribution by requiring at least one isolated track aligned with $\not\!\!E_T$ or 2 tracks having invariant mass within the Z Mass window. QCD and non-QCD background plus systematic uncertainties are shown.

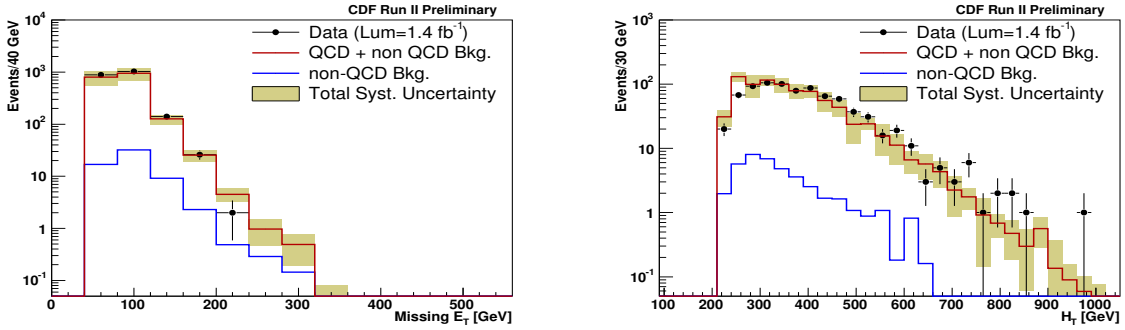

Figure 7: $\not\!\!E_T$ and H_T after all cuts in the 4-jet analysis except the $\not\!\!E_T$ and H_T cuts respectively, but reversing the $\Delta\phi(\not\!\!E_T, \text{jets})$ cut by asking at least one of the jets to fail the condition. QCD and non-QCD background plus systematic uncertainties are shown.

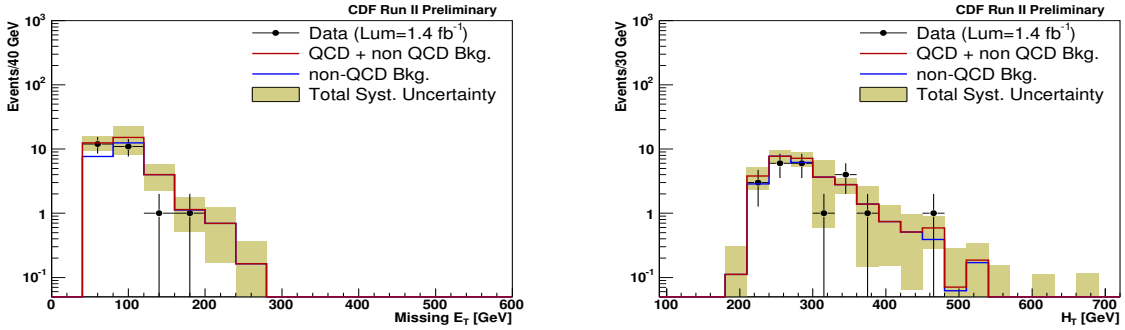

Figure 8: $\not\!\!E_T$ and H_T after all cuts in the 4-jet analysis except the $\not\!\!E_T$ and H_T cuts respectively, but reversing the EMF requirement by asking at least one of four leading jets to fail the condition. QCD and non-QCD background plus systematic uncertainties are shown.

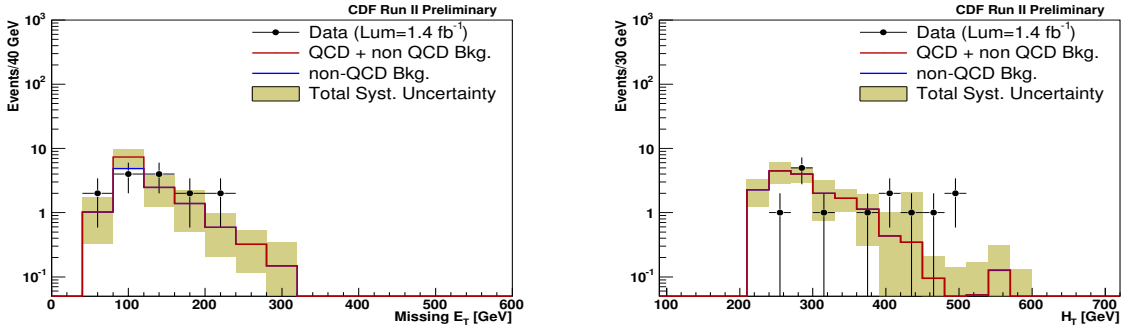

Figure 9: $\not\!\!E_T$ and H_T after all cuts in the 4-jet analysis except the $\not\!\!E_T$ and H_T cuts respectively, but enhancing the muon contribution by requiring at least one isolated track aligned with $\not\!\!E_T$ or 2 tracks having invariant mass within the Z Mass window. QCD and non-QCD background plus systematic uncertainties are shown.

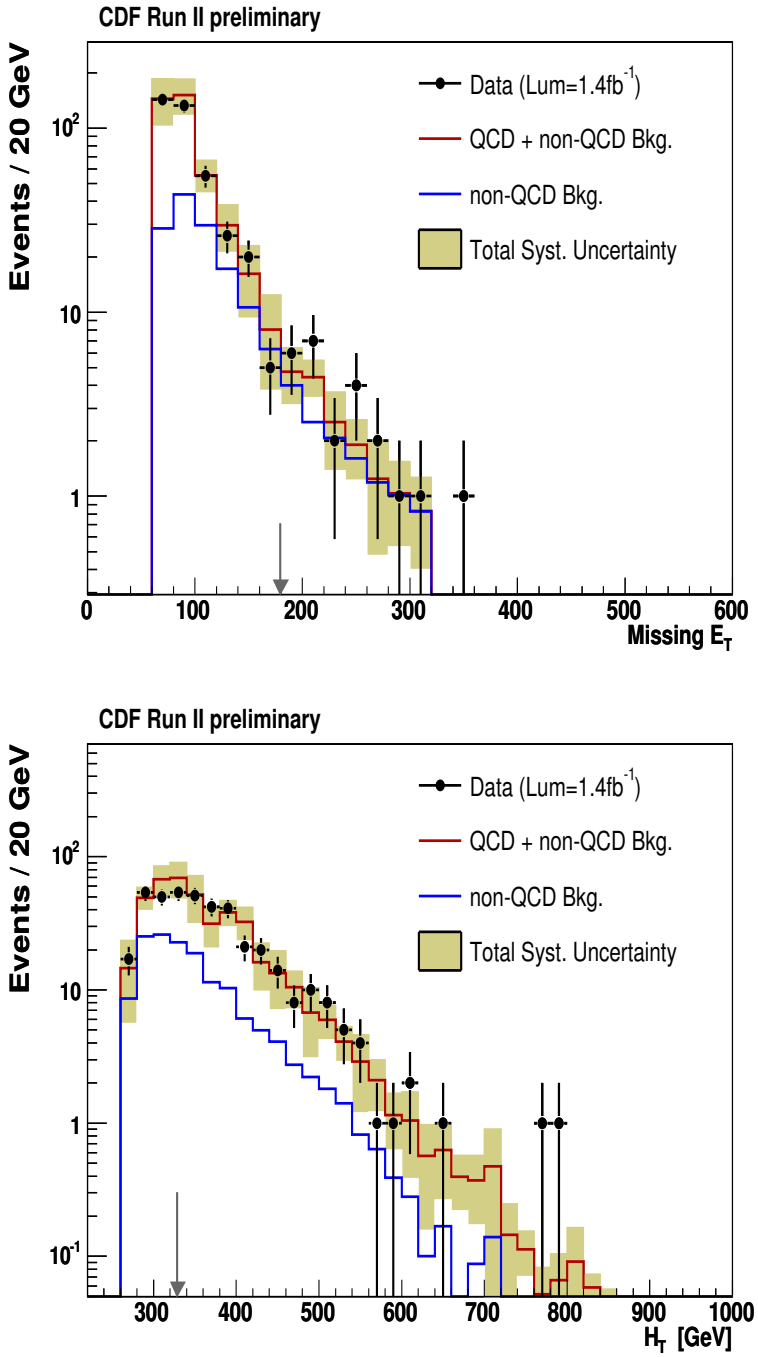

Figure 10: $\not\!\!E_T$ and H_T after all cuts in the 2-jet analysis except the $\not\!\!E_T$ and H_T cuts (N-2 plots). QCD and non-QCD background plus systematic uncertainties are shown.

2 Results and exclusion limit

The number of observed events and expected background are presented for a total integrated luminosity of 1373 pb^{-1}: they are reported in table 2, where results for the five selection regions are summerized. Systematic uncertainties on the background include 6% uncertainty on the luminosity.

Events in 1.4 fb^{-1}	Observed	**Total + statistics + systematics**
4-jets	29	$27 \pm 2 \pm 9$
3-jets(A)	616	$607 \pm 16 \pm 146$
3-jets(B)	166	$154 \pm 7 \pm 44$
3-jets(C)	22	$25 \pm 2 \pm 8$
2-jets	13	$11 \pm 2 \pm 3$

Table 2: Observed number of data events for the five selection regions in 1.4 fb^{-1}, compared with the expected events from SM Bkg.

Figures 11 to 15 show the H_T and $\not\!\!E_T$ distributions for the final results, for 3-jets (zones A, B, C), 2-jets and 4-jets regions. In these plots, all cuts have been applied except the one on the variable that is represented. Each figure shows the data together with the Monte Carlo predictions for the SM background. The background Monte Carlo predictions provide a reasonable description of the data and no excess with respect to the SM predictions is observed. For illustration purpose, one representative signal point is shown for the distributions of 3-jets (C), 2-jets and 4-jets regions, "stack" on top of the total background.

The final limit is extracted using, for each point, the selection that is giving the best expected limit, among the five selections defined as 2-jets, 4-jets and 3-jets.

Figures 16 to 19 show the evolution of the cross section values for two constant gluino masses[2]($M_{\tilde{g}} = 230$ GeV/c^2 and $M_{\tilde{g}} = 320$ GeV/c^2 respectively), for $M_{\tilde{g}} = M_{\tilde{q}}$ and for a constant squark mass ($M_{\tilde{q}} = 480$ GeV/c^2). Expected and observed limits are shown.

In figure 20 the exclusion region is reported: exclusion limits as determined by other experiments are also presented. In a mSUGRA scenario with $A_0 = 0$, $\mu < 0$ and $\tan\beta = 5$, we exclude masses up to about 380 GeV/c^2 (390 GeV/c^2 expected) at 95% C.L. in the region where gluino and squark masses are similar, gluino masses up to 280 GeV/c^2 for every squark mass, and gluino masses up to 410 GeV/c^2 for squark masses below 375 GeV/c^2.

In figure 21, a comparison with the exclusion limit as found by the DØ experiments in Run II[9] is reported.

The results of this analysis can be also used to constrain the mSUGRA parameters at the GUT scale. Figure 22 shows the excluded regions in the (m_0,$m_{1/2}$) plane for tanβ=5, A_0=0 and μ <0. Limits from LEP2 chargino and slepton searches are improved for m_0 values between 75 and 250 GeV and for $m_{1/2}$ values between 130 and 165 GeV.

The expected limit is finally computed considering 4.4 fb^{-1} of luminosity. In the projection, same relative systematic uncertainties on signal and background are assumed; the

[2]Squark and gluino masses implemented to compute the final results are the pole masses. Previously for this analysis, EWK masses were used. ΔM(pole-EWK) are found to be between 2 and 8 GeV/c^2 for gluinos, and between 10 and 20 GeV/c^2 for squarks. Both choices are theoretically correct, and the use of pole masses is mainly motivated by values currently used in other experiments.

number of signal and background events are rescaled by the luminosity factor. Figures 23 shows the evolution of the cross section values along the diagonal: the projections on the expected limit are superimposed to the current observed and expected limit. Figure 24 shows the squark-gluino mass plane with projections on the expected limit superimposed to the current observed and expected limit: squark and gluino masses (when $M_{\tilde{g}} = M_{\tilde{q}}$) are expected to be excluded up to 420 GeV/c^2 for 4.4 fb^{-1} of data.

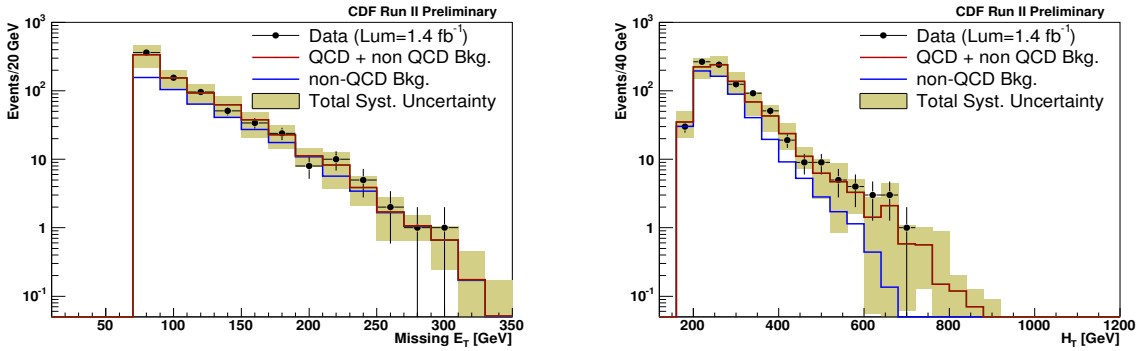

Figure 11: $\not\!\!E_T$ and H_T after all selection cuts for the 3-jet Zone A region: data are superimposed to QCD and non-QCD background with total systematics uncertainties. In these plots, all cuts have been applied except the one on the variable that is represented.

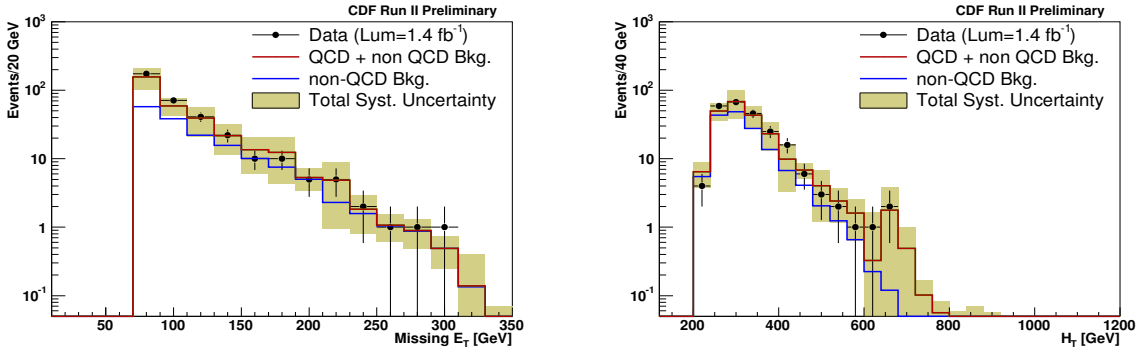

Figure 12: $\not\!\!E_T$ and H_T after all selection cuts for the 3-jet Zone B region: data are superimposed to QCD and non-QCD background with total systematics uncertainties. In these plots, all cuts have been applied except the one on the variable that is represented.

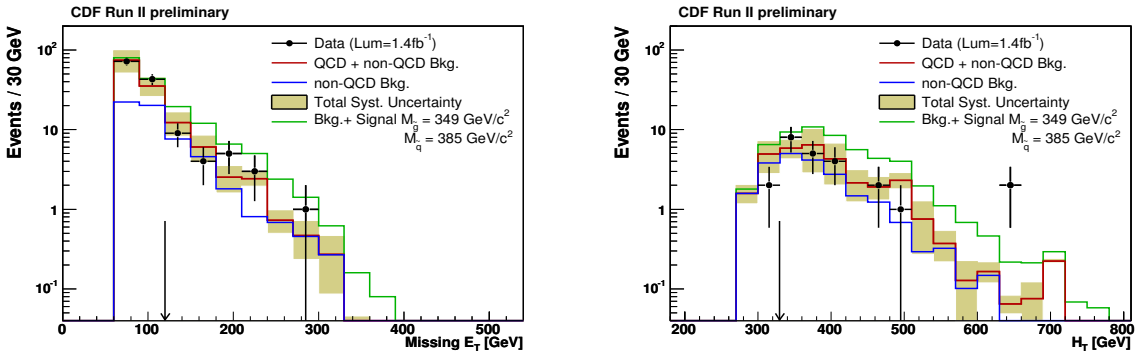

Figure 13: $\not\!\!E_T$ and H_T after all selection cuts for the 3-jet Zone C region: data are superimposed to QCD and non-QCD background with total systematics uncertainties. Distributions for a representative signal point is shown (stack). In these plots, all cuts have been applied except the one on the variable that is represented.

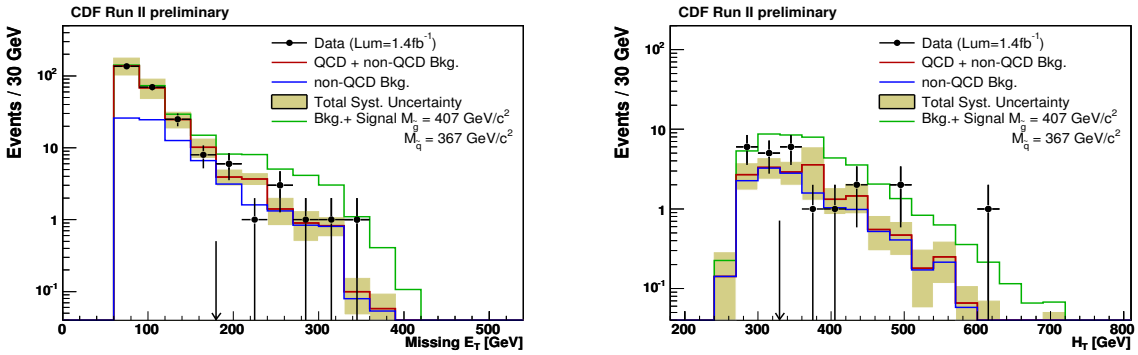

Figure 14: $\not\!\!E_T$ and H_T after all selection cuts for the 2-jet region: data are superimposed to QCD and non-QCD background with total systematics uncertainties. Distributions for a representative signal point is shown (stack). In these plots, all cuts have been applied except the one on the variable that is represented.

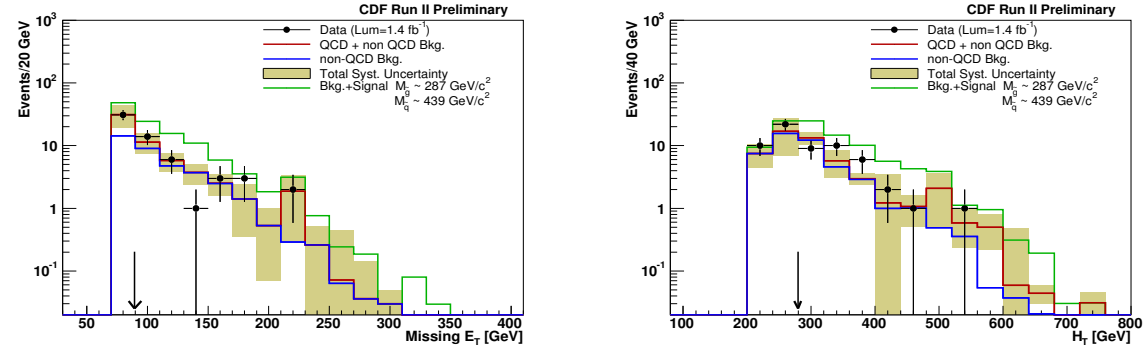

Figure 15: $\not\!\!E_T$ and H_T after all selection cuts for the 4-jet region: data are superimposed to QCD and non-QCD background with total systematics uncertainties. Distributions for a representative signal point is shown (stack). In these plots, all cuts have been applied except the one on the variable that is represented.

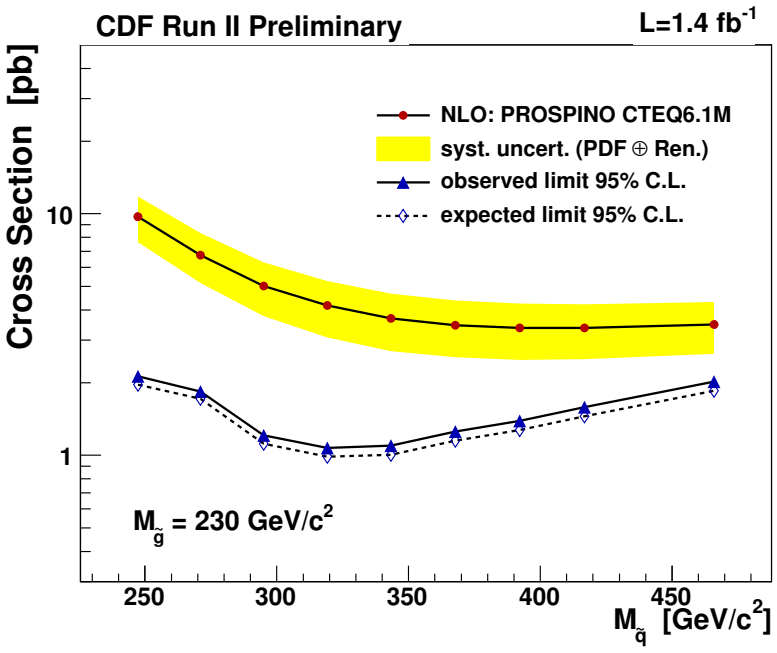

Figure 16: Cross section as a function of squark mass for $M_{\tilde{g}} = 230$ GeV/c^2. The observed and expected limits at 95% C.L. are shown. The yellow band shows the total effect of the PDFs and the renormalization scale uncertainties. In this case, squark masses are excluded up to arbitrarely high values.

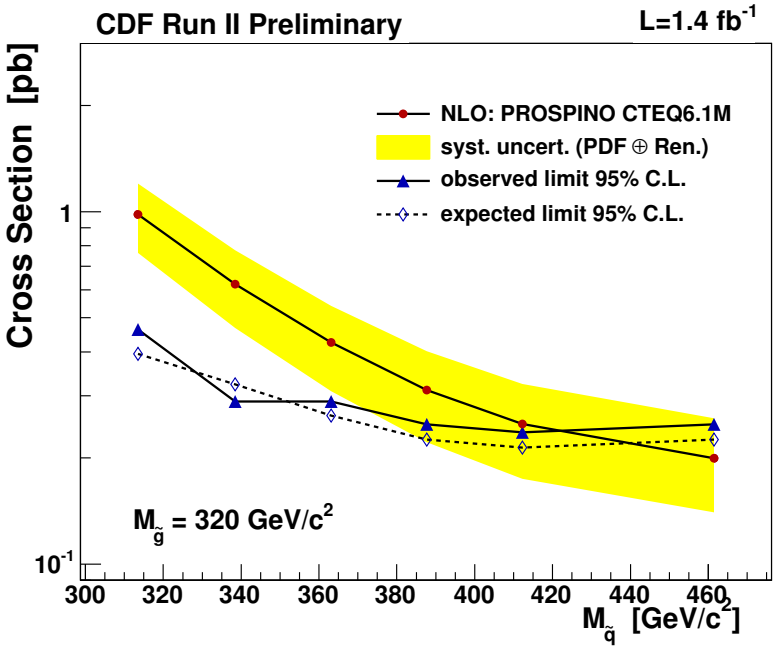

Figure 17: Cross section as a function of squark mass for $M_{\tilde{g}} = 320$ GeV/c^2. The observed and expected limits at 95% C.L. are shown. The yellow band shows the total effect of the PDFs and the renormalization scale uncertainties. Squark masses are excluded up to 425 GeV/c^2.

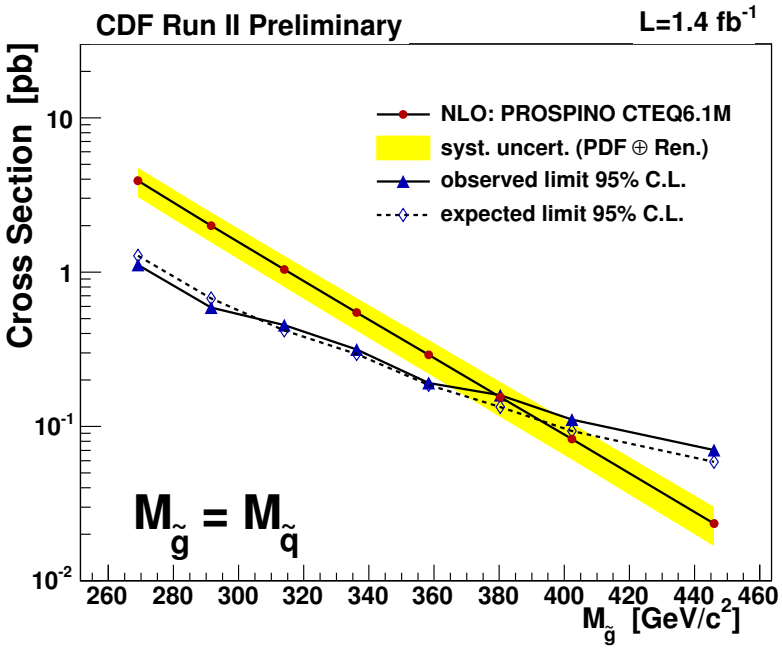

Figure 18: Cross section as a function of gluino/squark masses in the case of $M_{\tilde{q}} \approx M_{\tilde{g}}$ (diagonal). The observed and expected limits at 95% C.L. are also shown. The yellow band shows the total effect of the PDFs and the renormalization scale uncertainties. In this case, squark and gluino masses are excluded up to 380 GeV/c^2 (390 GeV/c^2 expected).

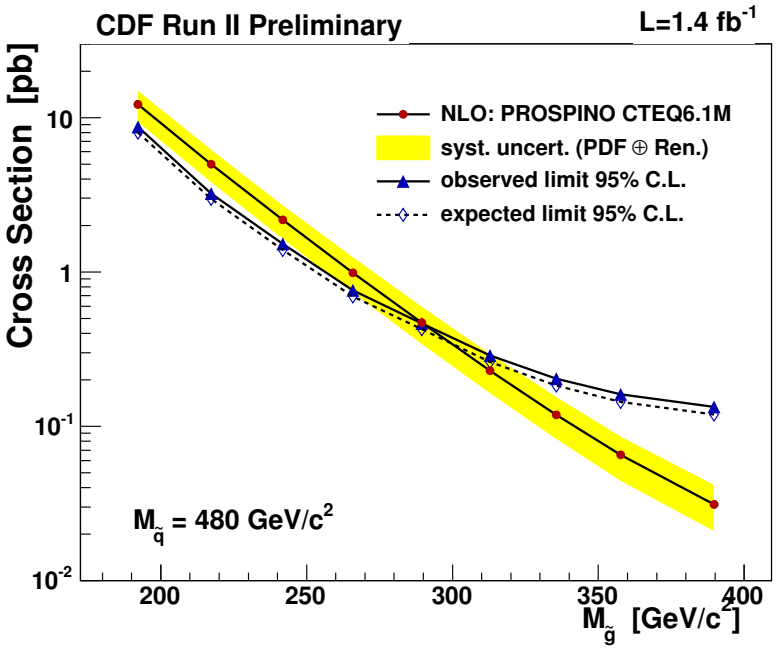

Figure 19: Cross section as a function of gluino mass for $M_{\tilde{q}} = 480$ GeV/c^2. The observed and expected limits at 95% C.L. are shown. The yellow band shows the total effect of the PDFs and the renormalization scale uncertainties.

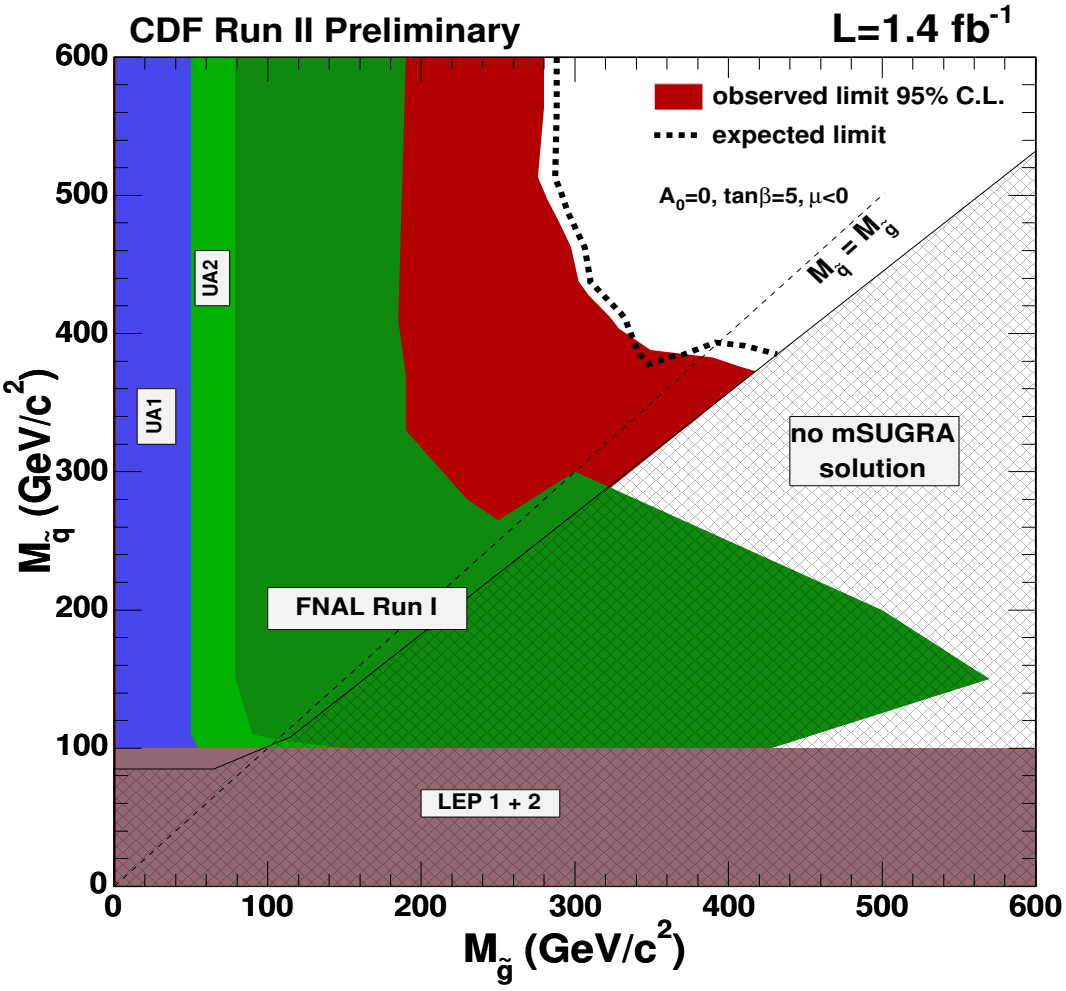

Figure 20: $M_{\tilde{q}}$ - $M_{\tilde{g}}$ exclusion plot at the 95 % C.L in the framework of mSUGRA assuming R-parity conservation. The blue region was excluded by the UA1 experiment [6]. The light-green region was excluded by the UA2 experiment [7]. The dark-green region was excluded by the CDF and DØ experiments after Run I [8]. The brown region was excluded by the LEP experiment [10]. In the black hashed region there is no mSUGRA solution. The dark-red region shows the area excluded by the current analysis with 1.4 fb^{-1} of CDF Run II data for the nominal cross section, including effects of the PDF uncertaintes and of varying the renormalization scale in the limit computation. The dashed black line shows the expected limit.

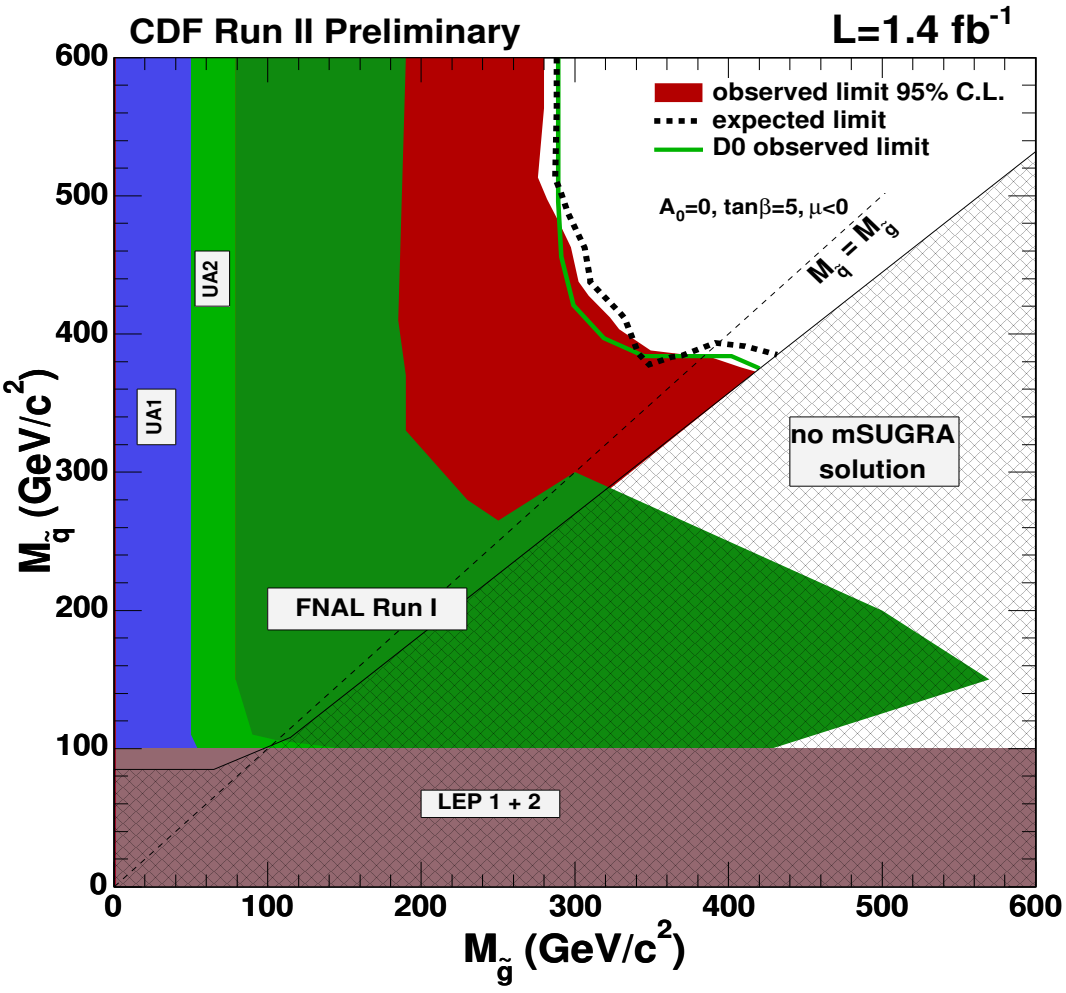

Figure 21: Same as figure 20, with region excluded by inclusive seaches performed by the DØ collaboration in Run II superimposed[9].

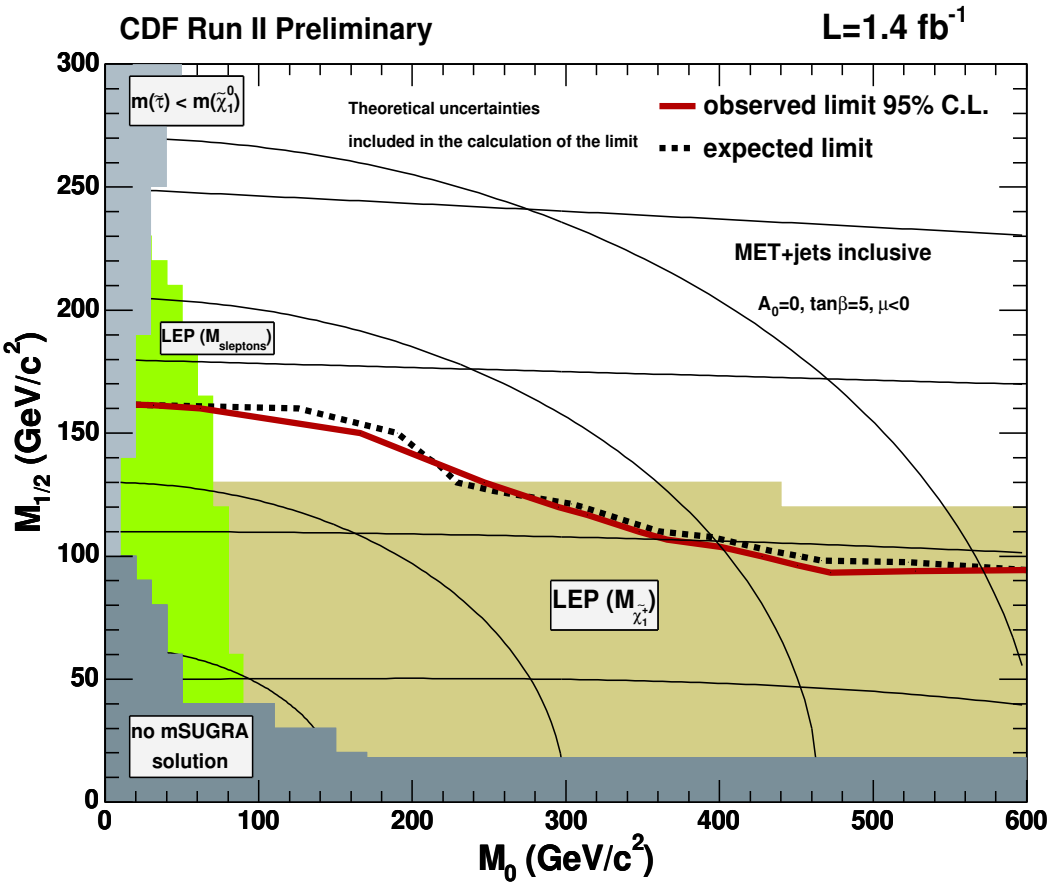

Figure 22: Regions excluded by this analysis at the 95% C.L. in the (m_0,$m_{1/2}$) plane, in the framework of mSUGRA assuming R-parity conservation, tanβ=5, A_0=0 and μ <0. In the dark-grey region there is no mSUGRA solution. The light-grey region indicates the region where $m(\tilde{\tau}) < m(\tilde{\chi}_1^0)$. The beige and green regions are excluded by LEP2 chargino and slepton searches[10], respectively. The nearly horizonthal black lines are the iso-mass curves for gluinos corresponding to masses of 150, 300, 450 and 600 GeV/c^2. The other lines are iso-mass curves for squarks, corresponding to masses of 150, 300, 450 and 600 GeV/c^2. The dark-red line shows the exclusion limit set by the current analysis with 1.4 fb^{-1} of CDF Run II data for the nominal cross section. The dashed black line shows the expected limit.

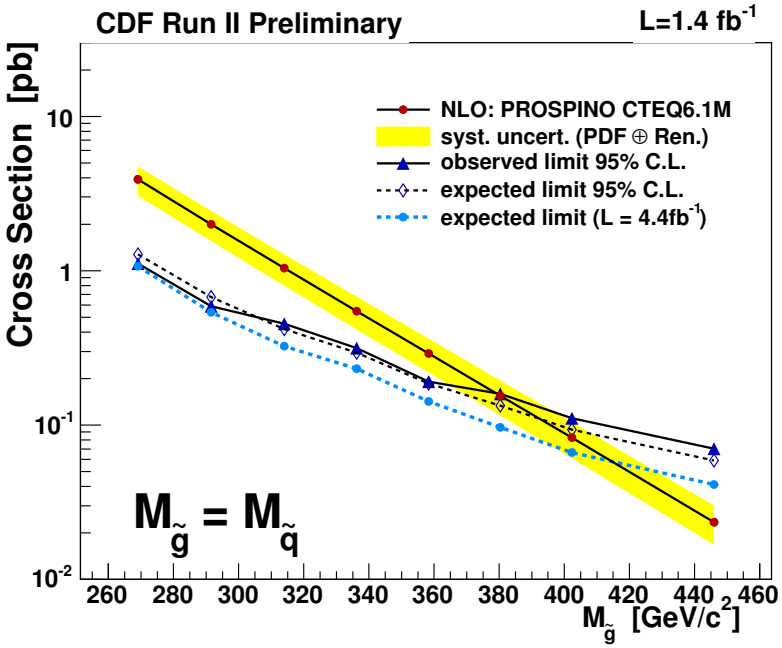

Figure 23: Cross section as a function of gluino/squark masses in the case of $M_{\tilde{q}} \approx M_{\tilde{g}}$ (diagonal). The observed and expected limits at 95% C.L. are also shown. The yellow band shows the total effect of the PDFs and the renormalization scale uncertainties. In this case, squark and gluino masses are excluded up to 380 GeV/c^2 (390 GeV/c^2 expected). The blue line shows the expected limit assuming the same analysis is performed with 4.4 fb^{-1} of data. Squark and gluino masses are expected to be excluded up to 420 GeV/c^2.

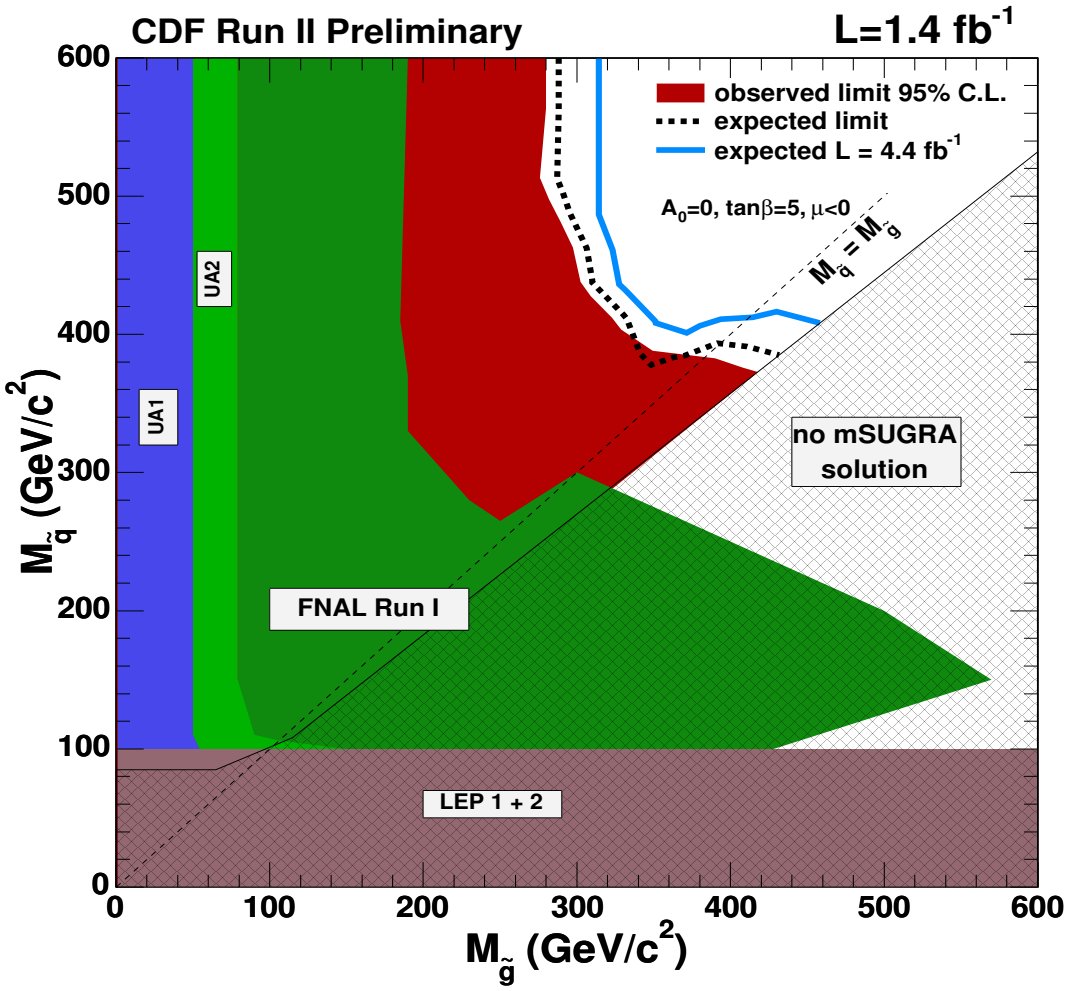

Figure 24: $M_{\tilde{q}}$ - $M_{\tilde{g}}$ exclusion plot at the 95 % C.L in the framework of mSUGRA assuming R-parity conservation. The blue region was excluded by the UA1 experiment [6]. The light-green region was excluded by the UA2 experiment [7]. The dark-green region was excluded by the CDF and DØ experiments after Run I [8]. The brown region was excluded by the LEP experiment [10]. In the black hashed region there is no mSUGRA solution. The dark-red region shows the area excluded by the current analysis with 1.4 fb^{-1} of CDF Run II data for the nominal cross section, including effects of the PDF uncertaintes and of varying the renormalization scale in the limit computation. The dashed black line shows the expected limit. The blue line shows the expected limits assuming the same analysis is performed with 4.4 fb^{-1} of data.

References

[1] cdfNote 8751.

[2] cdfNote 8885.

[3] http://www-cdf.fnal.gov/internal/physics/joint_physics/instructions/p8Problems.html.

[4] S. Klimenko *et al.*, FERMILAB-FN-0741 (2003); D. Acosta *et al.*, Nucl. Instrum. Meth. **A494**, 57 (2002).

[5] Joel Heinrich, CDF Note 7587.

[6] UA1 Collaboration, C. Albajar *et al.*, Phys. Lett. **B198** (1987) 261.

[7] UA2 Collaboration, S. Albachi *et al.*, Phys. Lett. **B235** (1990) 363.

[8] DØ Collaboration, B. Abbott *et al.*, Phys. Rev. Lett. **83** (1999) 4937. CDF Collaboration, T. Affolder *et al.*, Phys. Rev. Lett. **88** (2002) 041801.

[9] DØ Collaboration, P. Verdier, DØ Note 5312-CONF.

[10] The LEP-SUSY working group: *http://lepsusy.web.cern.ch/lepsusy/*